Optical Engineering 44(8), 083604 (August 2005)

Computer method for ELISA spot assay analysis

Chih-Yang Lin
Yu-Tai Ching
National Chiao Tung University
Department of Computer and Information Science
Hsin Chu, Taiwan

Betty A. Wu-Hsieh
National Taiwan University College of Medicine
Graduate Institute of Immunology
Taipei, Taiwan

Abstract. The ELISA (enzyme-linked immunosorbent assay) spot assay is a method widely used by immunologists to enumerate cytokine-producing cells within a specific cell population. The ELISA results are presented in an image containing numerous colored spots. We present a method to identify the spots in the image and report on important statistics regarding them. The proposed method employs color analysis in the CIE $L^*u^*v^*$ color space and matched filter technique. The system is trained to obtain a standard color for the spots and calculate the color differences between the spots and background in the $L^*u^*v^*$ space. Matched filters are then used to remove noise and enhance the spots in the color difference map. Intensity thresholding is applied to obtain a binary image in which the pixels in the spots have a grayscale of 1 while the grayscale of the other pixels is 0. A software system is implemented, based on this method, to help immunologists analyze the results obtained from the ELISA. © *2005 Society of Photo-Optical Instrumentation Engineers.* [DOI: 10.1117/1.2009767]

Subject terms: ELISA; spot; matched filter; segmentation; color analysis; CIE.

Paper 040189 received Apr. 2, 2004; revised manuscript received Dec. 1, 2004; accepted for publication Feb. 16, 2005; published online Aug. 10, 2005.

1 Introduction

The ELISA spot assay is designed to detect cells that produce cytokines.[1–3] Cytokines are proteins readily secreted by immune cells on stimulation by the antigens they recognize or by mitogens. The experimental steps are described as follows. Test wells are coated with anticytokine antibody (capturing antibody) before the cells are added. A certain number of cells and antigens are added to the precoated wells. During incubation the cells are stimulated to secrete cytokine. The precoated antibody captures the secreted cytokine. After washing, a biotinylated secondary anticytokine antibody (detecting antibody that recognizes different epitopes on the cytokine from the capturing antibody) and enzyme-avidin complex are added in sequence. A color reaction (red in this case) specific to cytokine-secreting cells occurs as a result of this enzymatic reaction. Each red spot represents one cytokine-secreting cell.

To analyze ELISA spot assay results, immunologists must know the numbers of spots, the distribution and size of the spots, and the mean and standard deviation of the spot sizes. Because these spots can number in the hundreds in each 70-mm-diameter well, counting the spots is labor-intensive work even when one uses a dissecting microscope. To overcome this problem, a computer method that helps immunologists calculate the important spot statistical values is needed.

Previous related work can be found in Refs. 4 and 5. In Ref. 4, an automatic method for particle detection from electron micrographs was proposed. A distance transform and the Voronoi diagram were used for detection of critical features as well as for accurate location of particles from the images or micrographs. The method could only find fixed-size disks. In our case, the size of spots is not fixed. In Ref. 6, an automatic circular decomposition algorithm applied to blood cell images was proposed. The method used polygonal approximation, curve segmentation, circle modeling, circle adapting, and circle merging to find various sizes of circles. The method needed edge detection as the first step for preprocessing. Unfortunately, in most of the cases, spots do not have obvious edges. In Ref. 7, automatic particle detection through efficient Hough transforms was proposed. The method could find various-size circles. But this method also needed edge detection before the Hough transform could be applied. In Ref. 5 a clustering-based method for particle detection is proposed. This method used gravitation to classify discrete points into a particle. It worked quite well for detecting particles from images with very low SNR. Before running the clustering algorithm, intensity thresholding is required. Since the boundaries for the spots are not clear, an appropriate threshold value is hard to determine.

In this paper, we present a method for ELISA spot assay analysis. The proposed method employs techniques that include illumination variation elimination, color analysis in

```
Find Spots(Image I) //Determine the spots in Image I;
{
    Eliminate illumination variation;
    Color space conversion;
    If (I is obtained from new experiment)
      Train the system to establish a standard color;
    Compute the color difference map;
    Enhance the spots using a matched filter;
    Identify the spots in image I;
}
```

Fig. 1 The pseudocode for the proposed method.

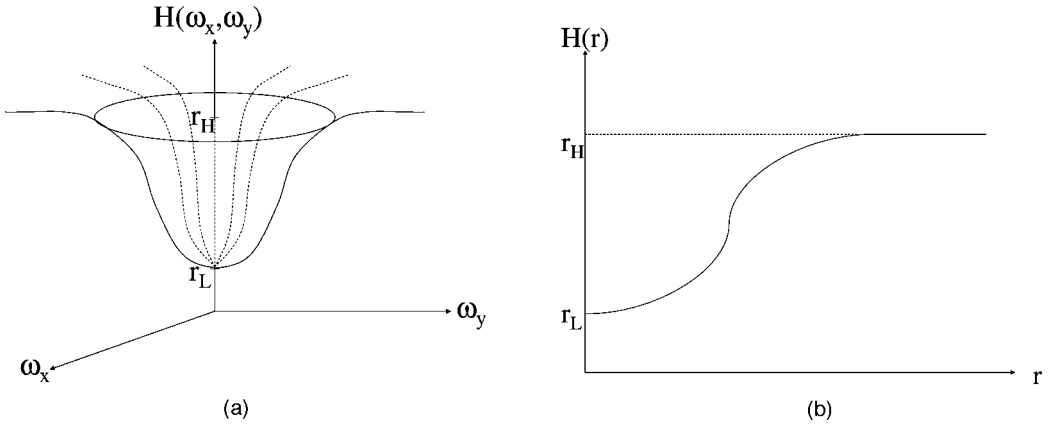

Fig. 2 (a) The high-pass filter spectrum. (b) A cross section of the high-pass filter as a function of the polar angle and frequency. In these figures $r=(\omega_x+\omega_y)^{1/2}$, $r_L=1/(1+e^{s\omega_0})$, and $r_H=1+A$.

the CIE $L^*u^*v^*$ color space, and matched filtering to enhance the spots in the image. After the preprocessing steps, intensity thresholding can effectively segment the spots in the image.

In this paper, the proposed method is presented in Sec. 2. In Sec. 3, we briefly describe the software developed for this method. The results are shown in Sec. 4, and the conclusions are in Sec. 5.

2 Method

The most fundamental task involves segmenting the red spots in the well. The proposed segmentation method is based on color analysis and the matched-filter technique. There are five steps in the method. The first step is image preprocessing. Because a light source cannot be placed on the top of the well, the illumination is not evenly distributed over the well surface. The preprocessing step eliminates illumination variations. The second step involves color-space conversion. The objective is to determine a uniform color space to linearize the perceptibility of color differences. The third step has two stages. The training stage involves training the system to recognize the color of the spots. In the recognition stage, a color difference map of the image is calculated according to the standard spot color. The fourth step applies a matched filter to identify the spots and remove the undesired noise in the color difference map. Intensity thresholding is then applied to obtain a binary image in which the pixels in the spots are depicted as 1 while the other pixels are depicted as 0. The pseudocode of our proposed method is shown in Fig. 1.

2.1 *Removal of Variable Illumination*

Variable illumination causes problems when the intensity threshold is applied. It is necessary to remove these illumination variations. Let $f(x,y)$ $(0\leqslant x\leqslant M-1, 0\leqslant y\leqslant N-1)$ denote an M-by-N spot image. Then $f(x,y)$ is the product of the reflectance $r(x,y)$ and the illumination $i(x,y)$[8]:

$$f(x,y)=i(x,y)r(x,y). \tag{1}$$

Suppose that the illumination is not evenly distributed over an image. The variation in illumination over the image consists of a low-frequency component in the frequency domain. Elimination of illumination variation is carried out using the following steps. We first use a logarithmic operation on both sides of Eq. (1) to obtain

$$\ln f(x,y)=\ln i(x,y)+\ln r(x,y). \tag{2}$$

Note that the right-hand side of Eq. (1) is transformed from multiplication to addition. We then transfer $\ln f(x,y)$ the frequency domain:

$$\ln F(m,n)=\sum_{x=0}^{M-1}\sum_{y=0}^{N-1}\ln f(x,y)\exp\left[-2\pi j\left(\frac{xm}{M}+\frac{yn}{N}\right)\right]. \tag{3}$$

In the frequency domain, a high pass filter is employed to suppress the low-frequency components. We then add a compensation operation back into the image to compensate for the suppressed signal. The high-pass filter,

$$H(\omega_x,\omega_y)=\frac{1}{1+\exp\{-s[(\omega_x^2+\omega_y^2)^{1/2}-\omega_0]\}}+A \tag{4}$$

suppresses the low frequencies and enhances the high frequencies so that the variation in the illumination can be reduced while the edges are sharpened. The response of $H(\omega_x,\omega_y)$ and its cross section are shown in Fig. 2.

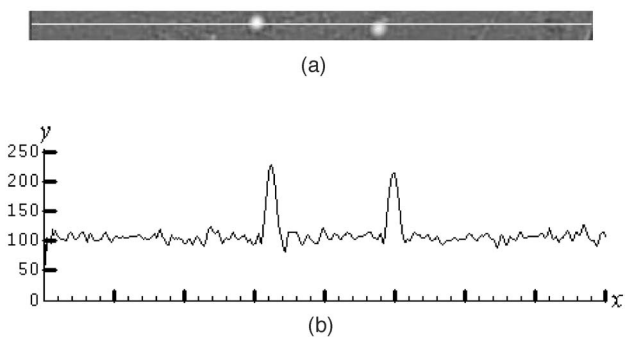

Fig. 3 (a) A portion of the color difference map. The white line denotes a cross section. (b) The gray-level profiles of the cross section in (a). The *x* coordinate denotes the pixels along the cross section. The *y* coordinate denotes the gray level.

-19	-19	-19	-19	-18	-18	-17	-17	-17	-16	-17	-17	-17	-18	-18	-19	-19	-19	-19	
-19	-19	-19	-18	-17	-16	-15	-14	-13	-13	-13	-14	-15	-16	-17	-18	-19	-19	-19	
-19	-19	-18	-17	-15	-13	-11	-9	-8	-7	-8	-9	-11	-13	-15	-17	-18	-19	-19	
-19	-18	-17	-15	-12	-9	-5	-2	0	1	0	-2	-5	-9	-12	-15	-17	-18	-19	
-18	-17	-15	-12	-8	-2	3	8	12	13	12	8	3	-2	-8	-12	-15	-17	-18	
-18	-16	-13	-9	-2	5	13	22	27	30	27	22	13	5	-2	-9	-13	-16	-18	
-17	-15	-11	-5	3	13	25	37	44	47	44	37	25	13	3	-5	-11	-15	-17	
-17	-14	-9	-2	8	22	37	50	60	64	60	50	37	22	8	-2	-9	-14	-17	
-17	-13	-8	0	12	27	44	60	71	75	71	60	44	27	12	0	-8	-13	-17	
-16	-13	-7	1	13	30	47	64	75	80	75	64	47	30	13	1	-7	-13	-16	
-17	-13	-8	0	12	27	44	60	71	75	71	60	44	27	12	0	-8	-13	-17	
-17	-14	-9	-2	8	22	37	50	60	64	60	50	37	22	8	-2	-9	-14	-17	
-17	-15	-11	-5	3	13	25	37	44	47	44	37	25	13	3	-5	-11	-15	-17	
-18	-16	-13	-9	-2	5	13	22	27	30	27	22	13	5	-2	-9	-13	-16	-18	
-18	-17	-15	-12	-8	-2	3	8	12	13	12	8	3	-2	-8	-12	-15	-17	-18	
-19	-18	-17	-15	-12	-9	-5	-2	0	1	0	-2	-5	-9	-12	-15	-17	-18	-19	
-19	-19	-18	-17	-15	-13	-11	-9	-8	-7	-8	-9	-11	-13	-15	-17	-18	-19	-19	
-19	-19	-19	-18	-17	-16	-15	-14	-13	-13	-13	-14	-15	-16	-17	-18	-19	-19	-19	
-19	-19	-19	-19	-18	-18	-17	-17	-17	-16	-17	-17	-17	-18	-18	-19	-19	-19	-19	

(a)

-23	-22	-22	-22	-22	-22	-22	-21	-21	-21	-20	-20	-19	-19	-19	-19	-18	-18	-18	-19	-19	-19	-19	-20	-20	-21	-21	-21	-22	-22	-22	-22	-22	-22	-23
-22	-22	-22	-22	-22	-22	-21	-21	-21	-20	-20	-19	-18	-18	-17	-17	-17	-17	-16	-17	-17	-17	-17	-18	-18	-19	-20	-20	-21	-21	-21	-22	-22	-22	-22	-22	
-22	-22	-22	-22	-22	-21	-21	-20	-20	-19	-18	-18	-17	-16	-15	-15	-14	-14	-14	-14	-14	-15	-15	-16	-17	-18	-18	-19	-20	-20	-21	-21	-22	-22	-22	-22	
-22	-22	-22	-22	-21	-21	-20	-19	-19	-18	-17	-16	-15	-14	-13	-12	-11	-11	-11	-11	-11	-12	-13	-14	-15	-16	-17	-18	-19	-19	-20	-21	-21	-22	-22	-22	
-22	-22	-21	-21	-20	-19	-18	-17	-16	-15	-13	-12	-10	-9	-8	-7	-7	-7	-7	-7	-8	-9	-10	-12	-13	-15	-16	-17	-18	-19	-20	-21	-21	-22	-22	-22	
-22	-21	-21	-20	-19	-18	-17	-16	-14	-12	-10	-8	-7	-5	-4	-3	-2	-2	-2	-3	-4	-5	-7	-8	-10	-12	-14	-16	-17	-18	-19	-20	-21	-21	-22	-22	
-22	-21	-20	-19	-18	-17	-15	-14	-11	-9	-7	-4	-2	0	1	2	3	3	3	2	1	0	-2	-4	-7	-9	-11	-14	-15	-17	-18	-19	-20	-21	-22	-22	
-21	-21	-20	-19	-17	-16	-14	-11	-9	-6	-3	0	2	5	7	9	10	10	10	9	7	5	2	0	-3	-6	-9	-11	-14	-16	-17	-19	-20	-21	-21		
-21	-20	-19	-18	-16	-14	-11	-9	-5	-2	1	4	8	11	14	16	17	18	17	16	14	11	8	4	1	-2	-5	-9	-11	-14	-16	-18	-19	-20	-21		
-21	-20	-18	-17	-15	-12	-9	-6	-2	1	6	10	14	18	22	24	26	26	26	24	22	18	14	10	6	1	-2	-6	-9	-12	-15	-17	-18	-20	-21		
-20	-19	-18	-16	-13	-10	-7	-3	1	6	11	16	21	26	30	33	34	35	34	33	30	26	21	16	11	6	1	-3	-7	-10	-13	-16	-18	-19	-20		
-20	-18	-17	-15	-12	-8	-4	0	4	10	16	22	28	33	38	41	43	44	43	41	38	33	28	22	16	10	4	0	-4	-8	-12	-15	-17	-18	-20		
-19	-18	-16	-14	-10	-7	-2	2	8	14	21	28	34	40	45	49	52	53	52	49	45	40	34	28	21	14	8	2	-2	-7	-10	-14	-16	-18	-19		
-19	-17	-15	-13	-9	-5	0	5	11	18	26	33	40	47	53	57	59	60	59	57	53	47	40	33	26	18	11	5	0	-5	-9	-13	-15	-17	-19		
-19	-17	-15	-12	-8	-4	1	7	14	22	30	38	45	53	59	63	66	67	66	63	59	53	45	38	30	22	14	7	1	-4	-8	-12	-15	-17	-19		
-19	-17	-14	-11	-7	-3	2	9	16	24	33	41	49	57	63	68	71	72	71	68	63	57	49	41	33	24	16	9	2	-3	-7	-11	-14	-17	-19		
-18	-17	-14	-11	-7	-2	3	10	17	26	34	43	52	59	66	71	74	75	74	71	66	59	52	43	34	26	17	10	3	-2	-7	-11	-14	-17	-18		
-18	-16	-14	-11	-7	-2	3	10	18	26	35	44	53	60	67	72	75	76	75	72	67	60	53	44	35	26	18	10	3	-2	-7	-11	-14	-16	-18		
-18	-17	-14	-11	-7	-2	3	10	17	26	34	43	52	59	66	71	74	75	74	71	66	59	52	43	34	26	17	10	3	-2	-7	-11	-14	-17	-18		
-19	-17	-14	-11	-7	-3	2	9	16	24	33	41	49	57	63	68	71	72	71	68	63	57	49	41	33	24	16	9	2	-3	-7	-11	-14	-17	-19		
-19	-17	-15	-12	-8	-4	1	7	14	22	30	38	45	53	59	63	66	67	66	63	59	53	45	38	30	22	14	7	1	-4	-8	-12	-15	-17	-19		
-19	-17	-15	-13	-9	-5	0	5	11	18	26	33	40	47	53	57	59	60	59	57	53	47	40	33	26	18	11	5	0	-5	-9	-13	-15	-17	-19		
-19	-18	-16	-14	-10	-7	-2	2	8	14	21	28	34	40	45	49	52	53	52	49	45	40	34	28	21	14	8	2	-2	-7	-10	-14	-16	-18	-19		
-20	-18	-17	-15	-12	-8	-4	0	4	10	16	22	28	33	38	41	43	44	43	41	38	33	28	22	16	10	4	0	-4	-8	-12	-15	-17	-18	-20		
-20	-19	-18	-16	-13	-10	-7	-3	1	6	11	16	21	26	30	33	34	35	34	33	30	26	21	16	11	6	1	-3	-7	-10	-13	-16	-18	-19	-20		
-21	-20	-18	-17	-15	-12	-9	-6	-2	1	6	10	14	18	22	24	26	26	26	24	22	18	14	10	6	1	-2	-6	-9	-12	-15	-17	-18	-20	-21		
-21	-20	-19	-18	-16	-14	-11	-9	-5	-2	1	4	8	11	14	16	17	18	17	16	14	11	8	4	1	-2	-5	-9	-11	-14	-16	-18	-19	-20	-21		
-21	-21	-20	-19	-17	-16	-14	-11	-9	-6	-3	0	2	5	7	9	10	10	10	9	7	5	2	0	-3	-6	-9	-11	-14	-16	-17	-19	-20	-21	-21		
-22	-21	-20	-19	-18	-17	-15	-14	-11	-9	-7	-4	-2	0	1	2	3	3	3	2	1	0	-2	-4	-7	-9	-11	-14	-15	-17	-18	-19	-20	-21	-22		
-22	-21	-21	-20	-19	-18	-17	-16	-14	-12	-10	-8	-7	-5	-4	-3	-2	-2	-2	-3	-4	-5	-7	-8	-10	-12	-14	-16	-17	-18	-19	-20	-21	-21	-22		
-22	-22	-21	-21	-20	-19	-18	-17	-16	-15	-13	-12	-10	-9	-8	-7	-7	-7	-7	-7	-8	-9	-10	-12	-13	-15	-16	-17	-18	-19	-20	-21	-21	-22	-22		
-22	-22	-22	-21	-21	-20	-19	-19	-18	-17	-16	-15	-14	-13	-12	-11	-11	-11	-11	-11	-12	-13	-14	-15	-16	-17	-18	-19	-19	-20	-21	-21	-22	-22	-22		
-22	-22	-22	-22	-21	-21	-20	-20	-19	-18	-18	-17	-16	-15	-15	-14	-14	-14	-14	-14	-15	-15	-16	-17	-18	-18	-19	-20	-20	-21	-21	-22	-22	-22	-22		
-22	-22	-22	-22	-22	-21	-21	-21	-20	-20	-19	-18	-18	-17	-17	-17	-17	-16	-17	-17	-17	-17	-18	-18	-19	-20	-20	-21	-21	-21	-22	-22	-22	-22	-22		
-23	-22	-22	-22	-22	-22	-22	-21	-21	-21	-20	-20	-19	-19	-19	-19	-18	-18	-18	-19	-19	-19	-19	-20	-20	-21	-21	-21	-22	-22	-22	-22	-22	-22	-23		

(b)

Fig. 4 Two-dimensional matched filters used in our proposed method. The radius is (a) 4 and (b) 8.

Because the spot edges contain high-frequency information and the illumination variations usually contain very low-frequency information, if the cutoff frequency of $H(\omega_x, \omega_y)$ is not too high, we can preserve the edge information and remove the illumination variation. We used 0.1 f_s as the cutoff frequency, where f_s is the sampling frequency. We have

$$A = 1 - \frac{1}{1 + e^{s\omega_0}}, \tag{5}$$

where ω_0 is the cutoff frequency and A is the compensation. Compensation is required because the high-pass filter has removed the low frequencies, including the dc term. The compensation A is automatically estimated by Eq. (5). Applying the high-pass filter (4) to In $F(m,n)$ yields

$$\ln F_i(m,n) = H(m,n)\ln F(m,n), \tag{6}$$

where $F_i(m,n)$ denotes the filtered image in the frequency domain.

The inverse Fourier transform is then applied:

$$\ln f_i(x,y) = \sum_{x=0}^{M-1}\sum_{y=0}^{N-1} \ln F_i(m,n)\exp\left[2\pi j\left(\frac{xm}{M} + \frac{yn}{N}\right)\right]. \tag{7}$$

Using an exponential operation restores the filtered signal.

2.2 *Color-Space Conversion*

The spots are extracted based on the differences between the colors of the spots and the background. A proper color space must be chosen before we can calculate the difference between colors. Over 40 color difference formulas were used before the CIE (Commission Internationale de I'Eclairage) recommended two standard color difference formulas, viz., the CIE $L^*a^*b^*$ and the CIE $L^*u^*v^*$, for surface and lighting industries.[9] These two formulas provide uniform color spaces. We chose the $L^*u^*v^*$ space.[10] Because video cameras use the *RGB* representation for colors, we converted the color representation from the *RGB* space into the $L^*u^*v^*$ space.[10] Before the coordinates in the $L^*u^*v^*$ space can be obtained, the representation from the *RGB* space must be converted into the *XYZ* space using

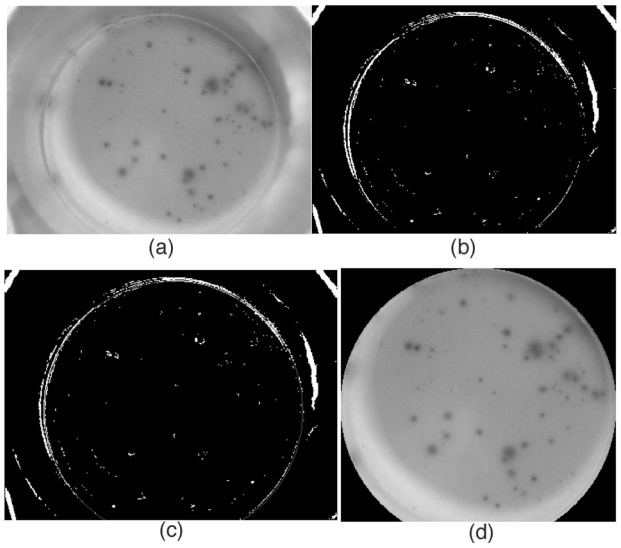

Fig. 5 (a) The original image. (b) Image after applying the Sobel filter. (c) After circle detection. (d) After removing the region outside the circle.

$$\begin{bmatrix} X \\ Y \\ Z \end{bmatrix} = \begin{bmatrix} 0.412453 & 0.357580 & 0.180423 \\ 0.412453 & 0.357580 & 0.180423 \\ 0.019334 & 0.119193 & 0.950227 \end{bmatrix} \begin{bmatrix} R \\ G \\ B \end{bmatrix}. \quad (8)$$

The $L^*u^*v^*$ space is based directly on the CIE XYZ. The nonlinear relations for L^*, u^*, v^*, X, Y, and Z are given below:

$$L^* = \begin{cases} 116(Y/Y)^{1/3} - 16 & \text{if } Y/Y_n > 0.008856, \\ 903.3(Y/Y_n) - 16 & \text{if } Y/Y_n \leq 0.008856, \end{cases} \quad (9)$$

$$u^* = 13L^*(u' - U'_n),$$

$$v^* = 13L^*(v' - v'_n). \quad (10)$$

In Eq. (10), (X_n, Y_n, Z_n) is the reference white in CIE XYZ; u', v', u'_n, and v'_n are given in the following equations:

$$u' = \frac{4X}{X + 15Y + 3Z},$$

$$v' = \frac{9Y}{X + 15Y + 3Z},$$

$$u'_n = \frac{4X_n}{X_n + 15Y_n + 3Z_n},$$

$$v'_n = \frac{9Y_n}{X_n + 15Y_n + 3Z_n}. \quad (11)$$

The daylight standard[9] D_{65} was used as the reference illuminant. The nonlinear relationship for Y is intended to mimic the logarithmic response of the eyes. The converted image in color space $L^*u^*v^*$ is denoted $f(x,y)_{L^*u^*v^*}$.

2.3 *Training the System and Obtaining an Image of the Color Differences*

To train the system to recognize a standard spot color, a user interface method is used to select an area $A(x,y)$ in the spot. Suppose there are N pixels in $A(x,y)$. The standard color $(\mu_{L^*}, \mu_{u^*}, \mu_{v^*})$ is obtained using the equations

$$\mu_{L^*} = [\sum A(x,y)_{L^*}]/N,$$

$$\mu_{u^*} = [\sum A(x,y)_{u^*}]/N,$$

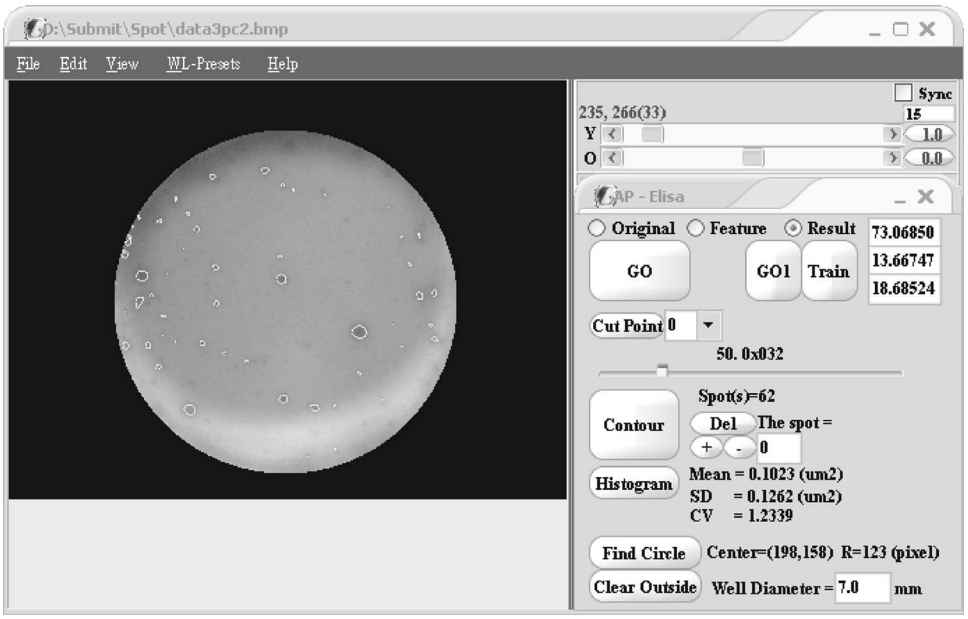

Fig. 6 A screenshot of the software system.

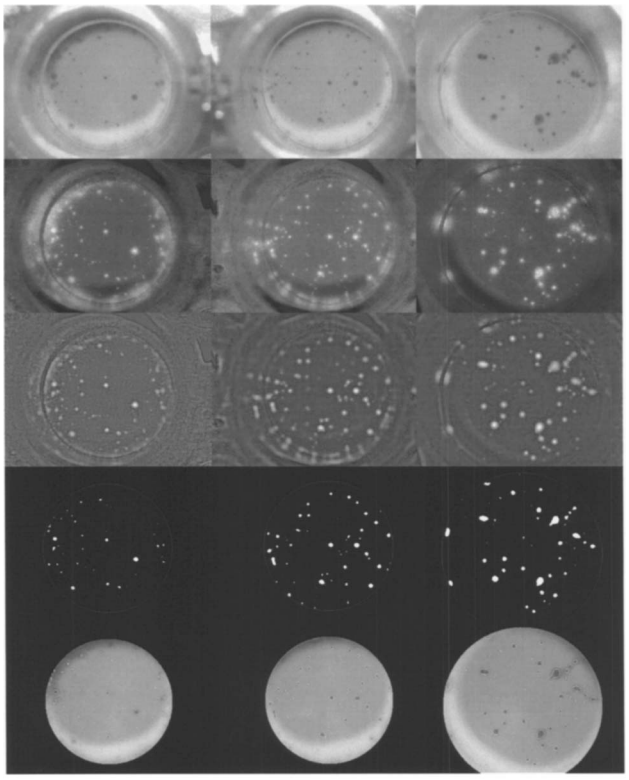

Fig. 7 First row: the three tested images from the proposed method. Second row: the color difference maps. In these images, the pixels with less difference are shown in the brighter intensity. Third row: the results after applying the matched filters. Fourth row: the final results. Fifth row: the original images overlying the results obtained in the images shown in the fourth row.

$$\mu_{v^*} = [\sum A(x,y)_{v^*}]/N. \tag{12}$$

The difference between the two measured colors in the CIE color difference formula is given by

$$\Delta E^*_{uv} = [(\Delta L^*)^2 + (\Delta u^*)^2 + (\Delta v^*)^2]^{0.5}. \tag{13}$$

Given an image $f(x,y)_{L^*u^*v^*}$ and a standard color $(\mu_{L^*}, \mu_{u^*}, \mu_{v^*})$, we can use Eq. (13) to obtain a color difference map $\Delta f(x,y)$, a grayscale image in which the differences between $f(x,y)_{L^*u^*v^*}$ and $(\mu_{L^*}, \mu_{u^*}, \mu_{v^*})$ are shown.

2.4 *Matched Filter for Spot Segmentation*

We used matched filters[11–14] to enhance the spots in the color difference map $\Delta f(x,y)$. As shown in Fig. 3, the shape of a spot in $\Delta f(x,y)$ is roughly a circle, and its gray-level profile of the cross section follows the Gaussian distribution. Indeed, the intensity profile of a spot nearly follows a two-dimensional Gaussian intensity distribution,[15] as shown in

$$g_1(x,y) = \exp[-(x^2+y^2)] = e^{-r^2}. \tag{14}$$

Here r is the radial distance measured from the center of a spot. If we define R as the radius at which the intensity drops to half its maximum value, we can rewrite the spot profile function as

$$g_1(x,y) = \exp[-(r/R)^2 \ln 2] = \exp[\ln(2^{-r^2/R^2})]. \tag{15}$$

Equation (15) can be simplified to obtain

$$g_1(x,y) = 2^{-(x^2+y^2)/R^2}. \tag{16}$$

To obtain a zero-mean filter, $g_1(x,y)$ is subtracted by m, the mean of the filter:

$$g(x,y) = g_1(x,y) - m = 2^{-(x^2+y^2)/R^2} - m. \tag{17}$$

Because the radii of different spots vary, we employed a set of different-size matched filters. The radii of the spots range between 4 and 16 pixels. We therefore used pixel sizes 4, 8, 12, and 16 as the radii to design the kernels of the matched filters. Figure 4 shows two of the four matched-filter kernels. After applying the matched filters to $\Delta f(x,y)$, most of the noise can be removed and the spots are enhanced.

2.5 *Computation of the Binary Image*

We set a threshold value for the resulting images. The threshold is determined either by the minimum-error thresholding method[16] or by the user intervening to decide a good threshold value. A binary image, in which the gray level for the pixels in the spots is depicted as 1 and the other pixels are depicted as 0, is obtained. The important statistical values are then derived from this binary image.

Before calculating the statistical values, we first compute the well regions. There are two reasons for doing so. The first is that the area outside the well is unwanted. Secondly, because we know that the well size is 7 mm, the pixel size can be derived from the segmented well region. Thus we are able to know the true sizes of the spots. We first convert the original image shown in Fig. 5(a) into a grayscale image and apply the Sobel filter[17] to the grayscale image. An edge map is obtained [Fig. 5(b)]. Applying the randomized algorithm for circle detection[18] to the edge

Table 1 The important statistical values.

Fig. 6 column	Well diam. (mm)	No. of spots	Mean (μm^2)	S.d. (μm^2)	CV
(a)	7.0	62	0.1023	0.1262	1.2339
(b)	7.0	70	0.1970	0.2120	1.0762
(c)	7.0	66	0.1989	0.2624	1.3188

Table 2 Comparison of inspection method and human inspection.

	No. of spots		
Fig. 6 column	Our method	Human count	Error (%)
(a)	62	63	1.5
(b)	70	71	1.4
(c)	66	68	2.9

map computes the well shown in Fig. 5(c). The area outside the circle is removed to obtain the region inside the well, shown in Fig. 5(d).

Finally, we segment the spots. Only the pixels in the well are considered. We compute the connected components formed by the pixels having value 1 after thresholding in the well. Each connected component is a spot. The size of the connected component is the size of the spot. The statistical values are then calculated.

3 A Software Tool

Based on the method described, we implemented a software system that provides a user-friendly interface for ELISA spot image analysis. A user can easily set experimental parameters such as the well diameter and the spot template. If the image intensity is too bright or too dark, the system provides window sliders to adjust the intensity and contrast. Because the colors of the spots vary between assays, the system provides a user interface method to establish the users' own customized parameters. Size-gated analysis (size filtering) enables a user to selectively count only the large spots. Other statistical analyses, such as calculating the standard deviation and the mean, are also provided. Figure 6 shows a screenshot of our software system.

4 Results

Several images were tested, and the results obtained using the proposed method is presented in this section. The input images were color images in BMP format of size 1600 by 1200 pixels, shown in the first row in Fig. 7. The images in the second row show the color difference maps. The results after applying the matched filtering are shown in the third row. The binary images after intensity thresholding are shown in the fourth row. The boundary points of the spots and the initial image are shown simultaneously in the fifth row. The well diameters in Fig. 7(a)–7(c) are 7.0 mm. The numbers of spots and other statistical values such as the mean, standard deviation, and coefficient of variance are shown in Table 1.

We evaluated the accuracy of the proposed computer method by comparing the numbers of spots identified by humans and the computer. Table 2 shows the results. A human could find more spots because humans can discern overlapping spots. The error rate was defined as the difference between the number of spots found and the number identified by a human. The error rates were less than 3% in our experiment.

The proposed methods were implemented on a PC with a Pentium 4 (2.2 GHz) CPU running on the Windows XP operating system. The overall execution time for a 1600 $\times$ 1200-pixel image was 5 s.

5 Conclusions

We have presented a computer method for ELISA spot analysis. The proposed method employs techniques such as color analysis and matched filtering to enhance the spots in the image. After preprocessing, intensity thresholding can effectively segment the spots. The experimental results showed that the error rate of the proposed method was less than 3%. This method can help immunologists to reduce the time in analyzing the ELISA spot assay. Since the errors occur when there are overlapping spots, in order to improve the accuracy, we hope to develop an intelligent method to separate the overlapping spots.

Acknowledgment

We thank Hsuen-Chin Chen for her technical support and helpful discussion. This work is supported under grant NSC-91-2213-E-009-076 by the National Science Council, Taiwan.

References

1. K. Fujihashi, J. R. McGhee, K. W. Beagley, D. T. McPherson, S. A. McPherson, C.-M. Huang, and H. Kiyono, "Cytokine-specific ELISPOT assay. Single cell analysis of IL-2, IL-4 and IL-6 producing cells," *J. Immunol. Methods* **160**, 181–189 (1993).
2. K. Murali-Krishna, J. D. Altman, M. Suresh, D. J. D. Sourdive, A. J. Zajac, J. D. Miller, J. Slansky, and R. Ahmed, "Counting antigen-specific CD8 T cells: A reevaluation of bystander activation during viral infection," *Immunity* **8**, 177–187 (1998).
3. A. Y. Karulin, M. D. Hesse, M. Tary-Lehmann, and P. V. Lehmann, "Single-cytokine-producing CD4 memory cells predominate in type 1 and type 2 immunity," *J. Immunol.* **164**, 1862–1872 (2000).
4. Z. Yu and C. Bajaj, "Detecting circular and rectangular particles based on geometric feature detection in electron micrographs," *J. Struct. Biol.* **145**, 168–180 (2004).
5. L. V. Guimaraes, A. A. Suzim, and J. Maeda, "A new automatic circular decomposition algorithm applied to blood cells image," in *1st IEEE Int. Symp. on Bioinformatics and Biomedical Engineering*, pp. 277–280 (2000).
6. Y. Zhu, "Automatic particle detection through efficient Hough transforms," *IEEE Trans. Med. Imaging* **22**(9), 1053–1062 (2003).
7. Z. Yu and C. Bajaj, "A clustering-based method for particle detection in electron micrographs," in *Fifth Int. Conf. on Advances in Pattern Recognition*, pp. 10–13, Indian Statistical Institute (2003).
8. P. Bosdogianni, *Image Processing—Fundamentals*, pp. 149–151, Wiley (1999).
9. Commission Internationale de l'Eclairage, *Colorimetry*, 2nd ed., CIE publ. 15.2, CIE, Paris (1986).
10. G. Wyszecki and W. S. Stiles, *Color Science: Concepts and Methods, Quantitative Data and Formulae*, 2nd ed., Wiley, New York, (1982).
11. S. Haykin, *Communication Systems*, Wiley Eastern, New Delhi, (1979).
12. D. H. Friedman, *Detection of Signals by Template Matching*, Johns Hopkins Univ. Press, Baltimore (1969).
13. G. L. Turin, "An introduction to matched filters," *IRE Trans. Inf. Theory* (Jun. 1960).
14. D. Middleton, "On new classes of matched filters and generalizations of the matched filter concept," *IRE Trans. Inf. Theory*, pp. 349–360, (Jun. 1960).
15. K. R. Castleman, *Digital Image Processing*, p. 41, Prentice Hall (1996).
16. J. R. Parker, *Algorithms for Image Processing and Computer Vision*, pp. 126–127, Willey Computer Publishing (1997).
17. L. S. Davis, "A survey of edge detection techniques," *Comput. Graph. Image Process.* **4**, 248–270 (1975).
18. T. C. Chen and K. L. Chung, "An efficient randomized algorithm for detection circles," *Comput. Vis. Image Underst.* **83**, 172–191 (2001).

Biographies and photographs of authors not available.